We are IntechOpen, the world's leading publisher of Open Access books Built by scientists, for scientists

4,800
Open access books available

122,000
International authors and editors

135M
Downloads

Our authors are among the

154
Countries delivered to

TOP 1%
most cited scientists

12.2%
Contributors from top 500 universities

CLARIVATE ANALYTICS BOOK CITATION INDEX INDEXED

WEB OF SCIENCE™

Selection of our books indexed in the Book Citation Index in Web of Science™ Core Collection (BKCI)

Interested in publishing with us?
Contact book.department@intechopen.com

Numbers displayed above are based on latest data collected.
For more information visit www.intechopen.com

14

Novel Space Exploration Technique for Analysing Planetary Atmospheres

George Dekoulis
Space Plasma Environment and Radio Science Group, Lancaster University
United Kingdom

1. Introduction

Spaceborne instrumentations impose strict design specifications for accurate and high-resolution magnetic field, ultraviolet, X-ray and stray light imaging power planetary measurements. Similar measurements can also be studied at suborbital altitudes. The various Space industries have expressed an interest over the recent years in providing capable suborbital instruments to complement current spaceborne activities. For instance, increasing the spatial resolution of a suborbital remote sensing instrument assists in better comprehending an in-situ measurement.

The various costs of employing cleanroom procedures, space qualification, launch and operation are in some cases reduced or eliminated. Costs associated to maintenance and upgrades are seriatim being reduced. High-resolution measurements rely on the design of noise-free, electromagnetic compatibility proof, multi-frequency, multi-bandwidth, multi-dynamic range and multi-integration time instrumentations. The frequency range of operation is selected to complement the bandwidths of spaceborne systems, in order to extend the limits of the various observations. In-situ data time-stamping, real-time clock support and geographical position ensure synchronisation to other networked data sets. Performing parametric alterations in run-time or automatic event-driven astrophysical observations demand programmable and dynamically reconfigurable instrumentations.

This chapter discusses the implementation of such specifications and presents the latest scientific results obtained from a novel radio interferometer system designed for galactic and extragalactic astrophysical studies. The system quantifies the planetary atmospheric layers' absorption of the energised galactic particle rays. The measurements are filtered from the Cosmic Microwave Background (CMB) and other last scattering surface cosmological emissions, which are post-processed independently.

Accurate right ascension and declination coordinates have determined the accuracy of measurements over existing radio interferometer systems. This is due to the strict specifications set early in the design process. The power and flexibility in terms of the available digital signal processing capacity is a virtue of the implemented hardware configuration. Heliospheric-driven events are sensed yielding to scientifically post-processed data products. The instrumentation is based in an all-digital reconfigurable

system architecture that satisfied the demands for various planetary atmospheric measurements.
The system is constantly being enriched by research results from an ongoing collaboration with NASA's Jet Propulsion Laboratory (JPL) on a different project for future missions. The presented system is complementary to existing and under development state-of-the-art systems, such as, interferometers, scalar/vector magnetometers etc. The system is a point of reference for seriatim high-resolution Deep Space missions with landing probes to Mars, Titan or Europa.

2. Space Observations

The CMB is the blackbody radiation left over from the Big Bang and has been the major source of scientific observations about the origin, geometry and constituents of the Universe for over 40 years. Blackbody radiation is emitted by an isothermal object that absorbs all incident radiation. The resulting radiation spectrum and the power received at a planet's surface, excluding frequency dependent atmospheric attenuation effects, depend on its temperature and can be calculated using the Planck function.
A large number of observations of the intensity of the CMB radiation have been made over the whole spectrum of available frequencies ranging from 0.5 MHz (Reber & Ellis, 1956) up to 10 THz (Braine & Hughes, 1999). Measurements have been made using spaceborne and suborbital experiments. Suborbital experiments include rocket-borne, balloon-borne (Mather et al., 1974) and ground-based instrumentations. Only a small percentage of the information available in the CMB has been captured to date.
The COsmic Background Explorer (COBE) mission was NASA's first CMB mission, outperforming any previous suborbital measurements in return-science. COBE was launched in 1989 and performed full sky observations until 1993. The spacecraft carried the Far-InfraRed Absolute Spectrophotometer (FIRAS) to search for radiation distortions, the Differential Microwave Radiometer (DMR) to study anisotropies and the Diffuse Infrared Background Experiment (DIBRE) (Kelsall et al., 1998).
The captured data proved that the CMB exhibits no deviations from a blackbody spectrum and the non-dipole anisotropy was determined. The absence of distortion from the spectrum and the detection of non-dipole anisotropy indicated that the large-scale geometry of the Universe must have been generated by dark matter gravitational forces. The gravitational forces were created during the first picosecond after the Big Bang. The anisotropy in sky power measurements indicated the interrelation between the seriatim evolved, although distant in time, Big Bang Nucleogenesis and Recombination eras. The two eras are separated by a factor of $10^{6.7}$ in cosmic scale.
NASA's currently active Wilkinson Microwave Anisotropy Probe (WMAP) mission was launched in 2001 to assist in establishing the initial conditions that existed at recombination (Bennett et al., 2003). Before recombination, ordinary matter was associated to photons, and structures like clusters of galaxies could not grow. After recombination, the clusters were able to expand and the measured data specify parameters related to the gravitational potential and density fluctuations at recombination. Knowledge of the initial conditions allows accurate determination of the behavior of the matter between the recombination era and now. Full sky observations occur in five frequency bands in the range 20-94 GHz, while the spacecraft is in an L2 orbit.

The European Space Agency (ESA) Planck mission to be launched in October 2008 is the third space mission after COBE and WMAP to study the anisotropies of the CMB radiation by scanning the whole sky at least twice. Planck will be placed in an L2 orbit. The spacecraft is equipped with the Low Frequency Instrument (LFI) and the High Frequency Instrument (HFI) to cover the frequency ranges 30-100 GHz and 100-857 GHz, respectively. Both instruments exhibit wide angular resolutions: 1980 arcsec at 30 GHz for the LFI being progressively improved to 300 arcsec at 857 GHz for the HFI. The angular resolution of the DMR was in the range of $\approx 7^{\circ}$. The LFI is an improved microwave radiometer, compared to DMR and WMAP, for the study of background anisotropies. The sensitivity of the HFI at the lower edge of the spectrum is close to the fundamental limit set by the photon statistics of the CMB itself (Lamarre et al., 2003).

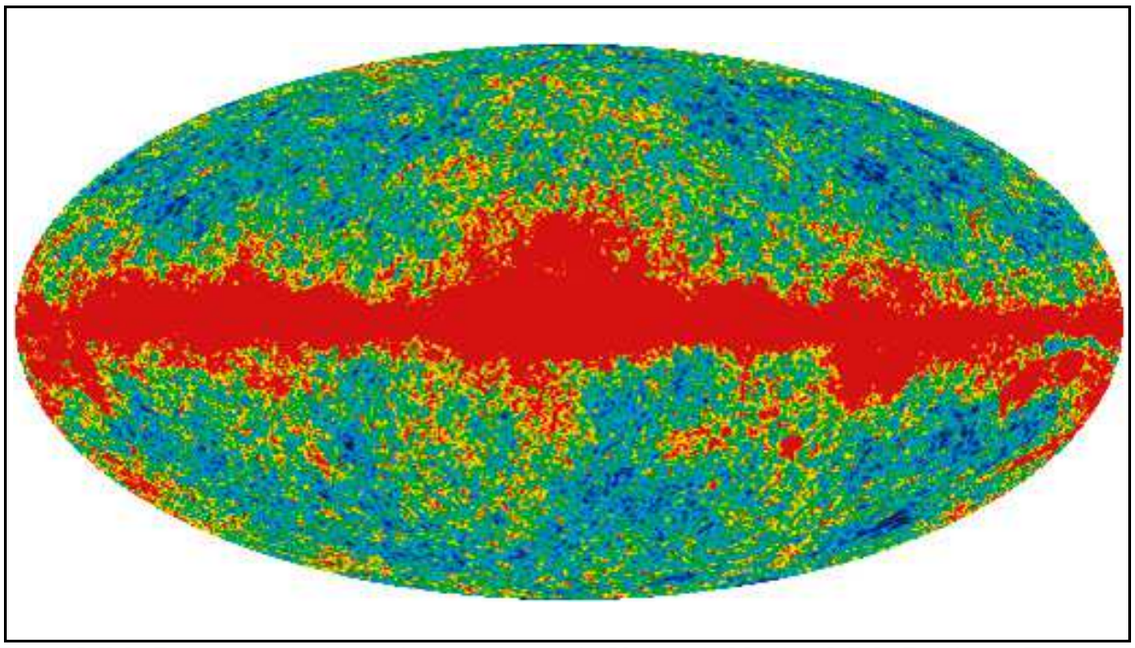

Fig. 1. WMAP sky map in Galactic coordinates in Ka band (NASA/WMAP Science Team).

Planck's observations would contribute significantly to measurements of fundamental cosmological parameters, such as the cold dark matter and baryon densities, with a maximum error of 1%. This would be possible, since hundreds of more points than COBE or WMAP on the angular CMB spectrum would be determined to allow a consistent check. An example of a five year temperature map at the Ka band for the WMAP is in Fig. 1 (Hinsaw et al., 2008). Similarly, measurements of space physics parameters at energies larger than 10^{15} GeV are not possible with any suborbital experiment.

However, the demands for capable suborbital and especially ground-based facilities have increased over the recent years. Costs associated with cleanroom procedures, space qualification, launch and operation are avoided. Low-cost ground instrumentations are easier to maintain and upgrade. Frequency ranges outside the bands of spaceborne instruments increase the range of scientific observations.

3. Wide-Beam Radio Interferometers Observing Attenuation

The CMB is the major source of the sky brightness at centimetre wavelengths. This corresponds to a temperature of 2.728 K and it is used to derive the brightness intensity of many other wavelengths in the near region (Wilson, 1979). Passive suborbital radio interferometers observing the sky at long radio wavelengths measure much brighter intensity than from the cosmic background alone. The corresponding effective temperature is >10,000 K at 33 MHz.

This radiation is due to highly energetic Galactic electrons, which radiate predominantly at those wavelengths. Their spectrum is different to the spectrum of the blackbody, safely assumed for the calculation of the different near-centimetre wavelengths cases, since the derivations do not include any radiation processes (Thomson et al., 2001). This is because radiation used to equipoise matter at an early cosmic evolution stage, and maintained its spectrum in any seriatim expansion and cooling stages.

Superimposed on the CMB radiation is any induced noise from the interferometer system itself. Including the emissions from the different radio stars at the frequency of observation, the system is still presented with very low-power levels to be measured. Some of these radio sources have angular sizes of several arcsec to be measured using narrow-beam radio interferometers at higher frequencies. Imaging systems use wide-beam antennas to deliberately exhibit resolution in the range of $\approx 11^{\circ}$/beam to cover wider sky areas. The strongest of these sources could be detected, if more directional antenna phased-array systems are built with higher spatial resolution for resolving the acquired power measurements. Introducing higher power gain systems is not an option, due to the passive nature of the systems.

In phased-array systems two strong radio sources are additionally superimposed on the background radiation. Due to the diurnal Earth's rotation first the extragalactic source Cygnus A and, then, the supernova remnant Cassiopeia A pass through the antenna-array field-of-view. Cygnus A radio galaxy is one of the strongest radio sky sources. The youngest supernova remnant in the Galaxy (300 years old) Cassiopeia A is the brightest radio source (Bell et al., 1975), although its emission is progressively decreasing.

The background radiation is attenuated as it passes through a planet's atmosphere. The amount of attenuation is mainly dependent to the frequency of observation. The order of the planet's idiomorphic magnetic field discriminates amongst the different atmospheric layers. The energy deposition mechanisms at different atmospheric altitudes, due to the solar wind's burst radiation and the precipitation of highly energetic particles, attenuate the background radiation before reaching the planet's surface. For Earth, the amount of attenuation is related to the activity of the complex solar wind–magnetospheric–ionospheric plasma environment. The vast three dimensional area of the solar-terrestrial plasma environment, still, has been partially sampled despite the numerous in-situ and suborbital observations. PLANCK will experience the streaming solar wind, magnetosheath, magnetospheric lobes and auroral tail plasmas in an L2 orbit, while the halo orbit places the spacecraft in the magnetosheath for long periods of time.

Fig. 2. Northern hemisphere survey of wide-beam systems.

At atmospheric altitudes where electron motion is collision-dominated, the partial release of the CMB radiation energy to heat through electron collisions signifies attenuation (Stoker et al., 1997). Atmospheric attenuation measurements depend on the frequency, geographic position, altitude, heliospheric activity and plasma ionisation mechanisms. Although solar wind radiation dominates planetary plasma ionisation during daytime, especially for the planets of the inner solar system, galactic energetic particles with energies between up to one hundred KeV sustain plasma density, ionisation and attenuation to a seasonal periodic level during night time.

Typically low-noise and sensitive receivers are used equipped with calibration circuits. Amplitude and, in some systems, phase, is measured of the received background wavefront. A single vertical antenna with the main lobe in the direction of local zenith can form a wide-beam system. The background radiation attenuation varies according to the Earth rotation, but remains constant for a repeated local sidereal time. Wide-beam systems with a single antenna above a ground plane have been reported to operate at frequencies of 16.6, 20, 20.5, 21.3, 25, 27.6, 29.7, 29.9, 30, 32, 32.4, 35, 38.2 and 51.4 MHz and bandwidths of 15 to 250 KHz (Abdu et al., 1967). At frequencies below 20 MHz the background radiation can be attenuated completely by the magnetospheric plasma without reaching Earth's surface. For frequencies over 50 MHz, the atmospheric attenuation is virtually un-differentiable from the CMB.

Known systems located in the northern and southern hemispheres are marked with red in Fig. 2 and 3, respectively. The antenna is usually a wide-beam design of a vertical three element Yagi, two parallel horizontal dipoles or a circularly polarised cross-dipole with a

beam-width in the region of 60°. Circularly polarised cross-dipole antennas receive both vertically and horizontally polarised transmitted radio signals. They are insensitive to plane polarisation variation due to the ionospheric Faraday rotation effect and are also used in L-band space observations (Le Vine & Abraham, 2004).

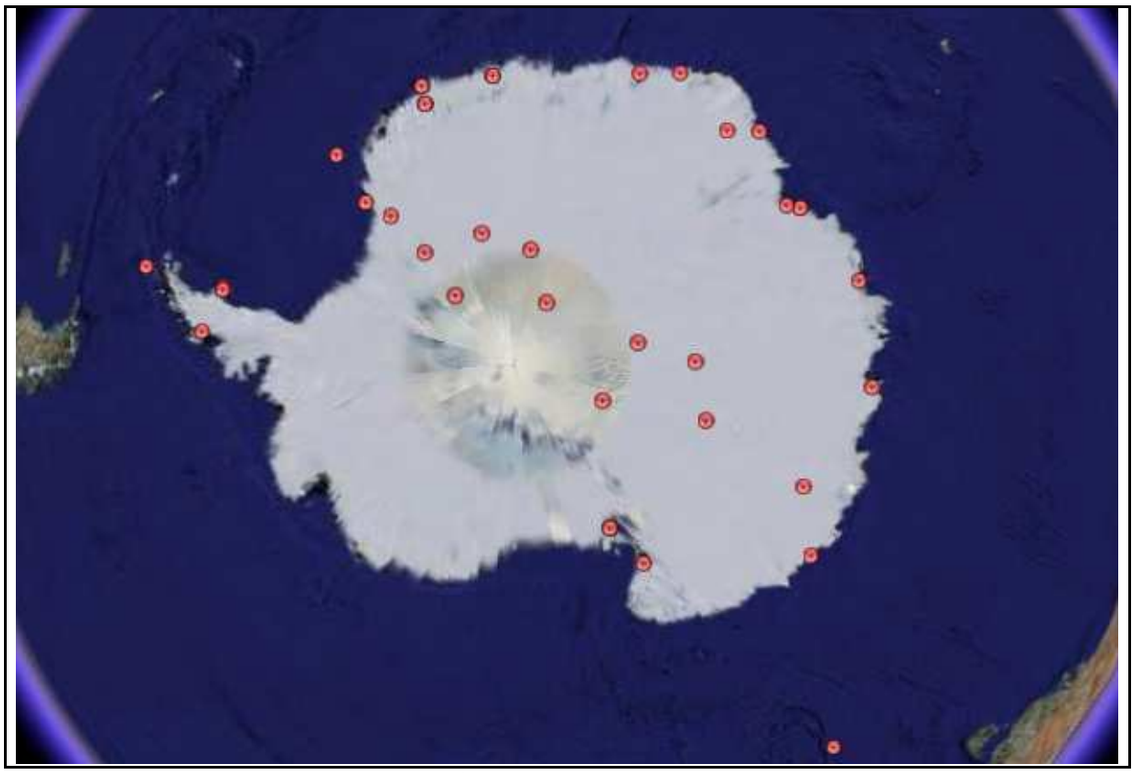

Fig. 3. Southern hemisphere survey of wide-beam systems.

Most of the systems installed in both northern and southern hemispheres have been built upon the principle of operation described in (Haldoupis et al., 1982). The design is based on the implementation of a feedback control loop to stabilise the output power, as shown in Fig. 4. The receiver continuously adjusts the noise source to match the power signal received by the antenna. A servo-controlled noise diode is typically used. The receiver input alternates between the antenna input and calibration noise source at a frequency rate of 583 Hz. The switching frequency is derived from a local oscillator. The difference between the antenna power and the noise diode signal is detected as a squarewave at 583 Hz. The squarewave is amplified and detected by the phase detector.

The output voltage of the detector is proportional to the mismatching and its polarity depends on the strongest signal. The output voltage is being used to adjust the power of the noise diode, in order to match the noise power of the antenna. The resulting difference is zero. The power of the noise diode is proportional to the current passing through it and the received power signal of the antenna is measured on a linear scale by recording the diode current.

The frequency of operation is typically determined as a function of geographical position and can vary according to the expected attenuation. At high-latitudes, and especially to

regions close to the polar cap, many systems have been operated at 27.6 MHz, since the corresponding attenuation is high. At lower geographical latitudes, 18 and 20 MHz have been traditionally used (Pinto & Gonzalez, 1989). Most of the recently installed systems, either at the northern or southern hemispheres, operate at 30 MHz.
The systems have been based upon the standard dual-stage superheterodyne receiver architecture. To avoid radio-wave interference at these frequencies, a swept-frequency and minimum-signal-detector scheme has been implemented. The first-stage local oscillator varies the frequency in 100 KHz steps every 40 s. The triangular frequency sweep is achieved by mechanically adjusting a capacitor determining the frequency of the first oscillator.

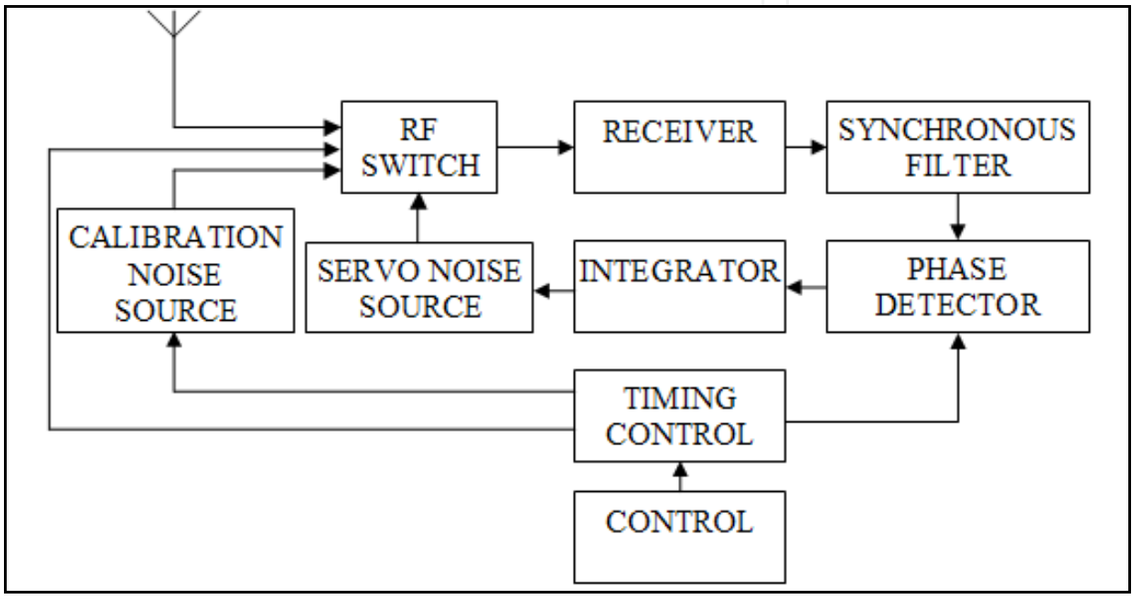

Fig. 4. Typical wide-beam system architecture.

Modern system architectures and digital signal processing technologies have carefully been considered and the optimum has been selected (Pui-In et al., 2007). The proposed system architecture mainly eliminates the classical analogue feedback control loop, exhibits an improvement in the overall performance by at least 9 dB and introduces state-of-the-art features and specifications into this field of science. The signal processing accuracy is increased. The scientific post-processing of the data also yields to more stable results.

4. Novel Wide-Beam Radio Interferometer

The new wide-beam system has been designed in a modular hardware and software manner, so that the high-speed field programmable gate array (FPGA) and host instrumentation are independent of the antenna type being used. In order to validate the advanced specifications set at the beginning of the project, a circularly polarised crossed-dipole antenna was designed, tuned to 38.2 MHz.
The system is capable of processing CMB emissions up to 60 MHz by electronically switching to the appropriate channel. Although attenuation measurements have been typically performed tuned to a single operating frequency in the range 25-50 MHz, the

system provides systematic coverage of CMB attenuation for a wide range of observations and environments. The power stabilising loop of Fig. 4 has been removed. The system is continuously monitoring the antenna input and exhibits improvement of 3 dB, in terms of power levels.

Frequency	1 - 60 MHz
Bandwidth	5 KHz - 1 MHz
Noise figure	3.05 dB
Sampling resolution	14 bits
Dynamic range	< 175 dB
Radiation protection	< SRE IV
Integration time	1 ms - 22 m
Tx losses	0 dB
ISA	> 300
Timekeeping	GPS (UTC) & RTC
GPS Recovery	Automatic
Onboard storage	< 144 h
Interfaces	RS-232, USB 2.0, 10/100 Mbps Fast Ethernet
Attenuation calculation	Automatic
Calibration	Automatic

Table 1. Specifications

The system amplifies the broadband input up to 60 MHz by 31.7 dB. The signal is further bandpass filtered to 1 MHz. The FPGA-controlled and custom-built digital amplifier (DA) takes into account the current Space Physics event being measured and adjusts the gain to a known level suitable for the analogue-to-digital converter (ADC) to detect. The ADC samples at 2.5 times the selected input. Investigation was made whether the signal can be processed at RF by the FPGA. The implementation results indicated that 400 clock cycles are required to produce the first result, excessive amount of hardware resources and raises the system cost significantly.

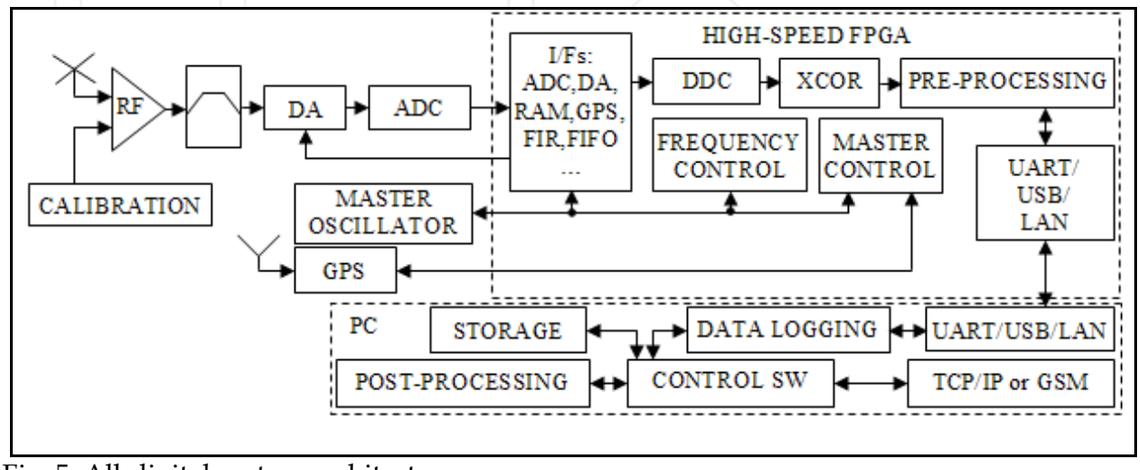

Fig. 5. All-digital system architecture.

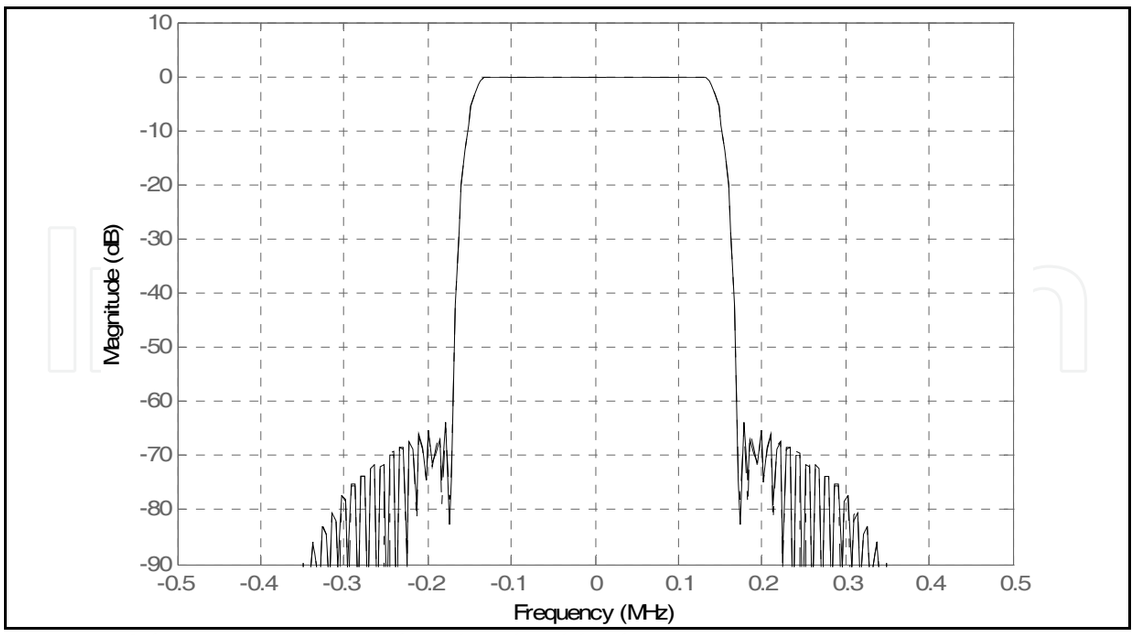

Fig. 6. DDC frequency response for a bandwidth of 250 KHz.

The FPGA-embedded digital-down-converter (DDC) converts the signal to baseband, reduces the data rate by a factor of 256 and extracts the in-phase (I) and quadrature (Q) components of the signal. The signal is low-pass filtered to the desired bandwidth. Fig. 6 demonstrates performance for a bandwidth of 250 KHz. The power results are integrated for a default 1 s and logged for post-processing. The programmable GPS receiver provides the pulse-per-second (PPS) signal, universal time (UT) for timestamping and geographic position for the theoretical calculation of the CMB radiation attenuation. A real-time clock (RTC) scheme has been implemented to allow the system's auto-recovery from loss of synchronisation. The system automatically computes attenuation by comparing the measured with the theoretical values.

The major new specifications introduced into this field of science are in Table 1. Most of the parameters are either reprogrammable or set via reconfiguration of the system. The new all-digital system architecture is presented in the block diagram of Fig. 5.

5. Scientific Results

The distributed FPGA data can be accessed by privileged PC hosts via the selected interface. The data are stored for post-processing. Data logging, programming and reconfiguration of the system favoured the usage of the 10/100 Mbps fast Ethernet interface during all phases of the testing. Using default settings and integration of the power results for 1 s, each sidereal day is represented by 86,164 UTC timestamped data values. The integrated power results are converted to dBm. The post-processing algorithms used are compatible with other networked data sets used by the SPEARS group at Lancaster University. Theoretical quiet day curves (QDCs) are derived knowing the CMB emissions, antenna radiation pattern and geographical location.

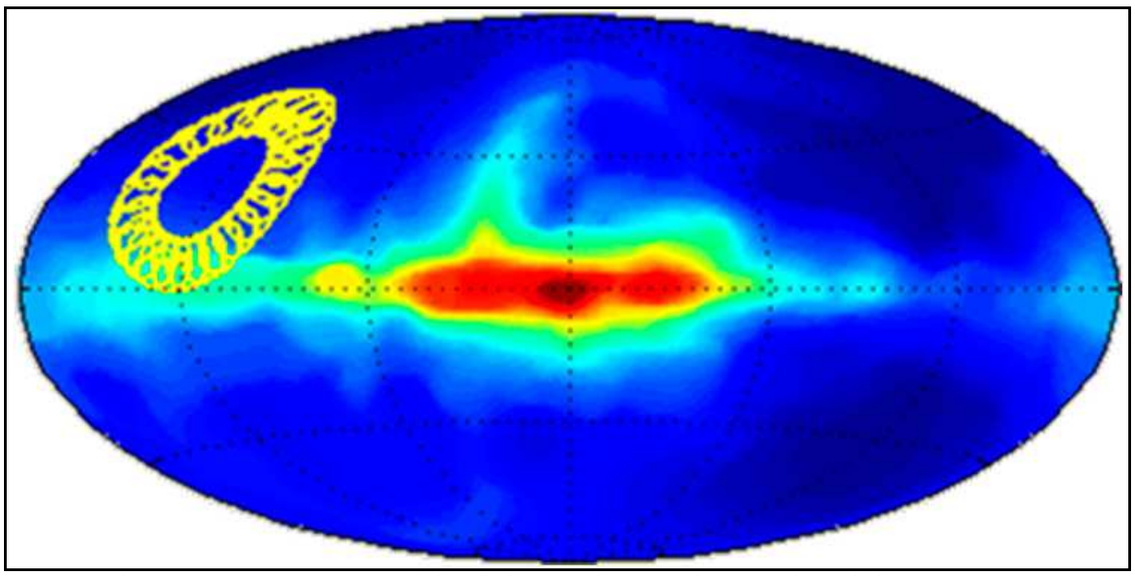

Fig. 7. Right ascension scanning of the Galactic plane within a sidereal day at 38.2 MHz.

A sky map in Galactic coordinates has been produced in Fig. 7 at 38.2 MHz. The cross-dipole antenna's field-of-view is projected at an altitude of 90 km, as shown in Fig. 8. CMB radiation attenuation is maximised at this altitude for the Earth environment. Similar results can be produced for any antenna type, knowing the current geographical position. The comparison between the experimental and theoretical CMB emissions for a quiet sidereal day is in Fig. 9. The corresponding attenuation is minimum and less than 0.1 dB, as shown in Fig. 10.

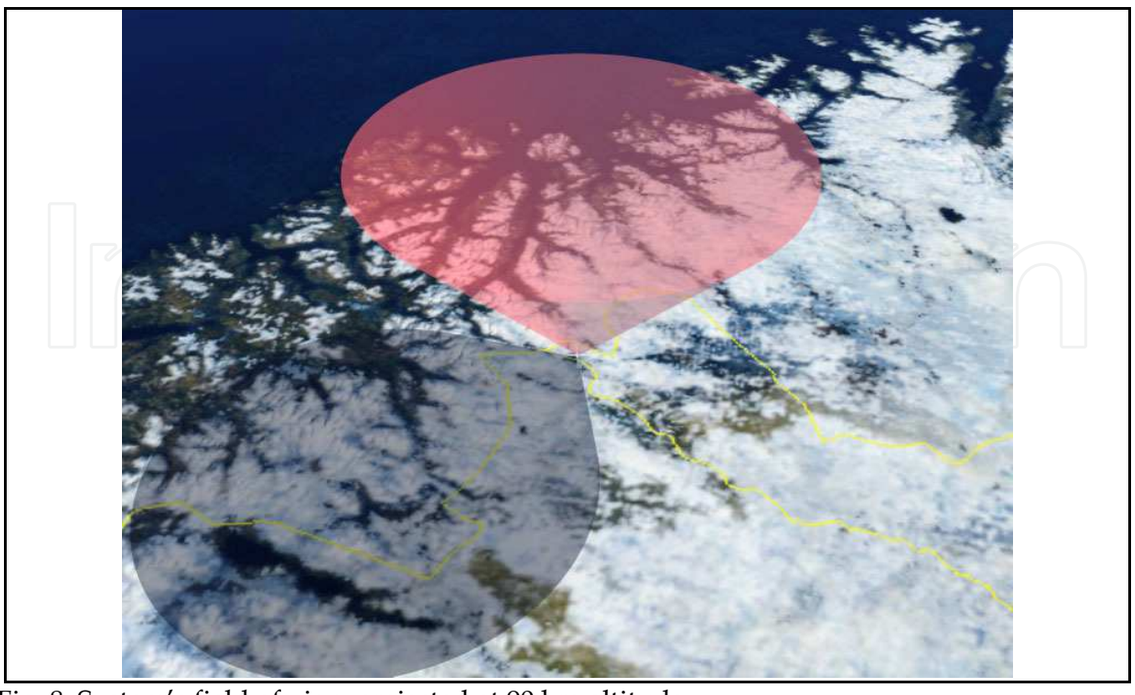

Fig. 8. System's field of view projected at 90 km altitude.

For Earth and Mars, attenuation A, is calculated in dB by solving the integral of eq. (1) and (2), respectively (Hargreaves, 1995; Rzhiga, 2005).

$$A = 1.14\times10^{5}\int dy\,\frac{n(y)}{v_c(y)}C_{5/2}\left(\frac{\omega\pm\Omega(y)}{v_c(y)}\right) \tag{1}$$

$$A = 4.62\times10^{4}\int dy\,\frac{1.5n(y)v_c(y)}{(1.5v_c(y))^2+\omega^2} \tag{2}$$

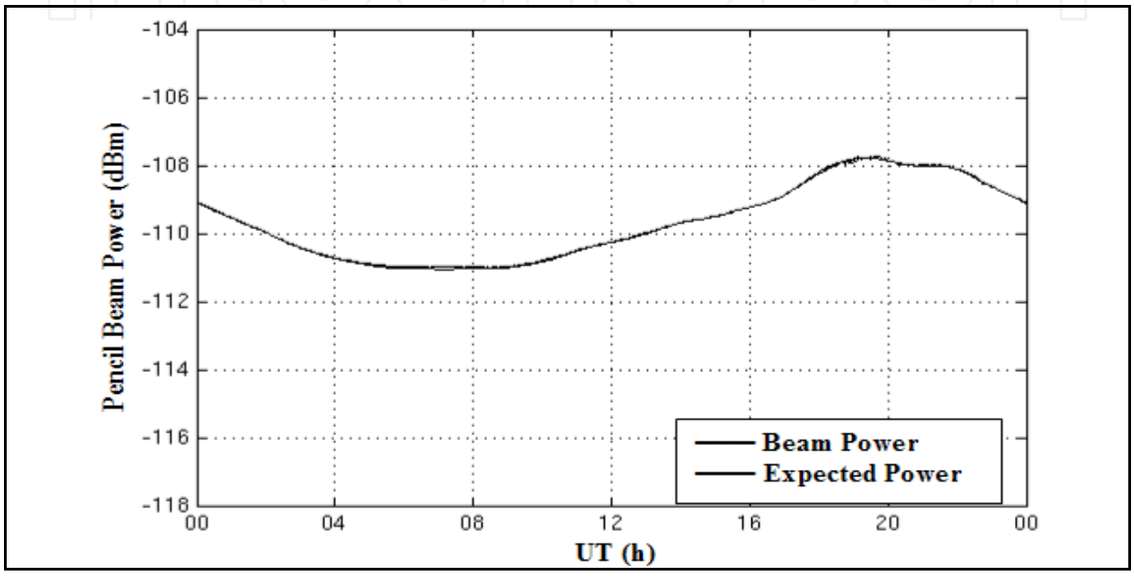

Fig. 9. Comparison between the received (RX) and expected (QDC) background emissions over a quiet sidereal day.

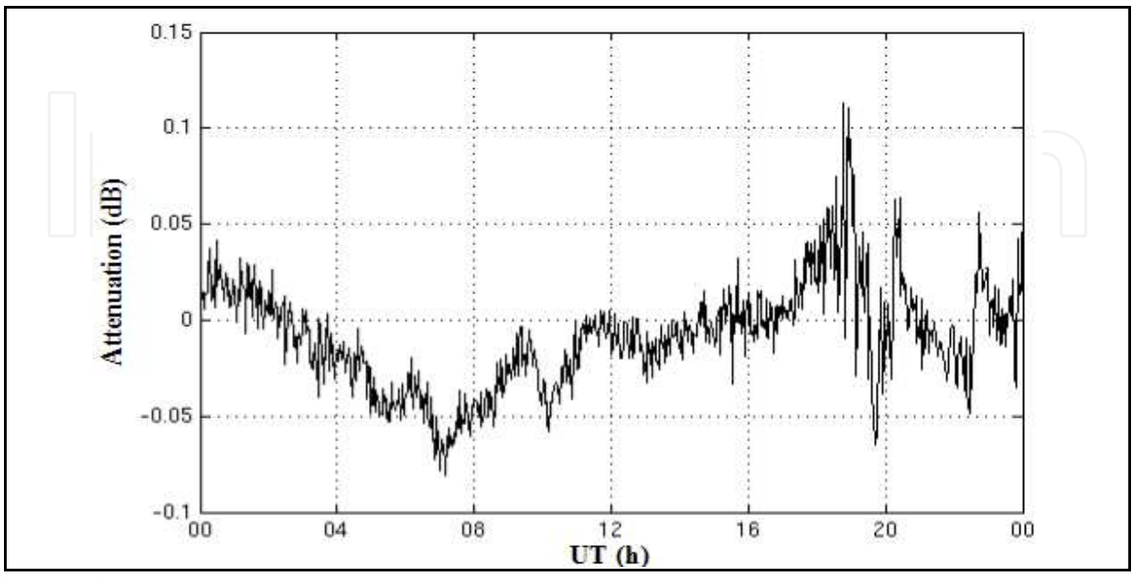

Fig. 10. Background attenuation for a quiet sidereal day.

where, y is the altitude variation of the electron-neutral momentum transfer collision frequency, $v_c(y)$ and electron plasma density, n(y), while ω is the system's angular frequency of observation, $C_{5/2}$ the semiconductor integral and $\Omega(y)$ the electron gyrofrequency. The instrument is being used to study a variety of heliospheric events as being measured on the planet's surface. For instance, abrupt solar flares cause sudden attenuation events detectable at medium and high frequencies, as in Fig. 11. The corresponding sudden attenuation is in Fig. 12.

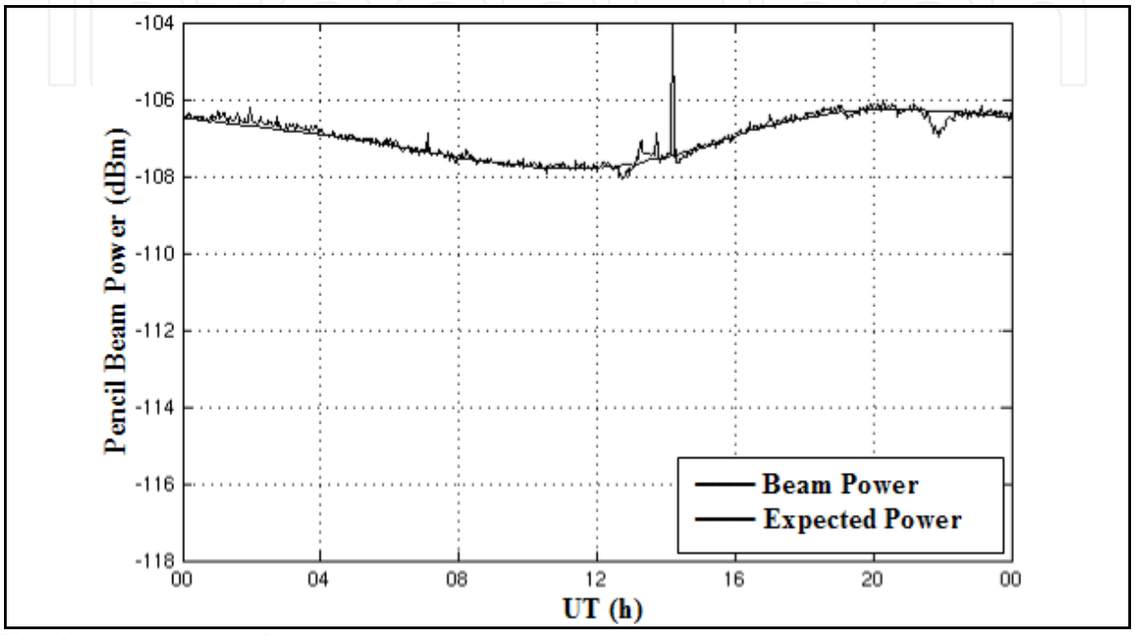

Fig. 11. Abrupt solar flare.

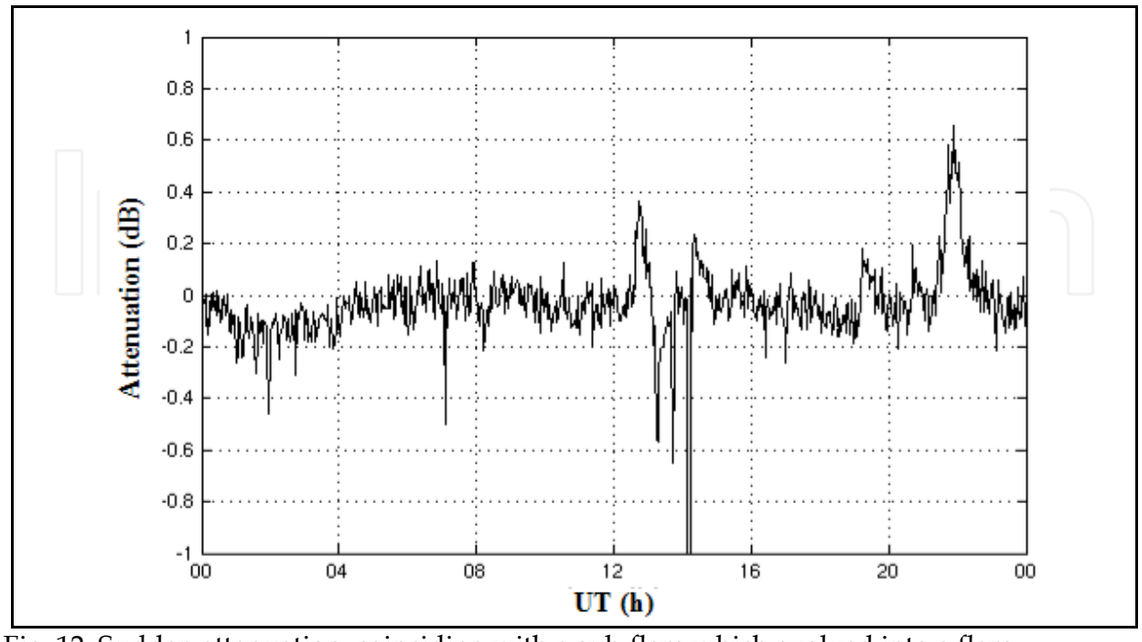

Fig. 12. Sudden attenuation, coinciding with a sub-flare which evolved into a flare.

The event coincided with a sub-flare, which evolved into a flare from SGR 1900+14 in Fig. 13 and 14.

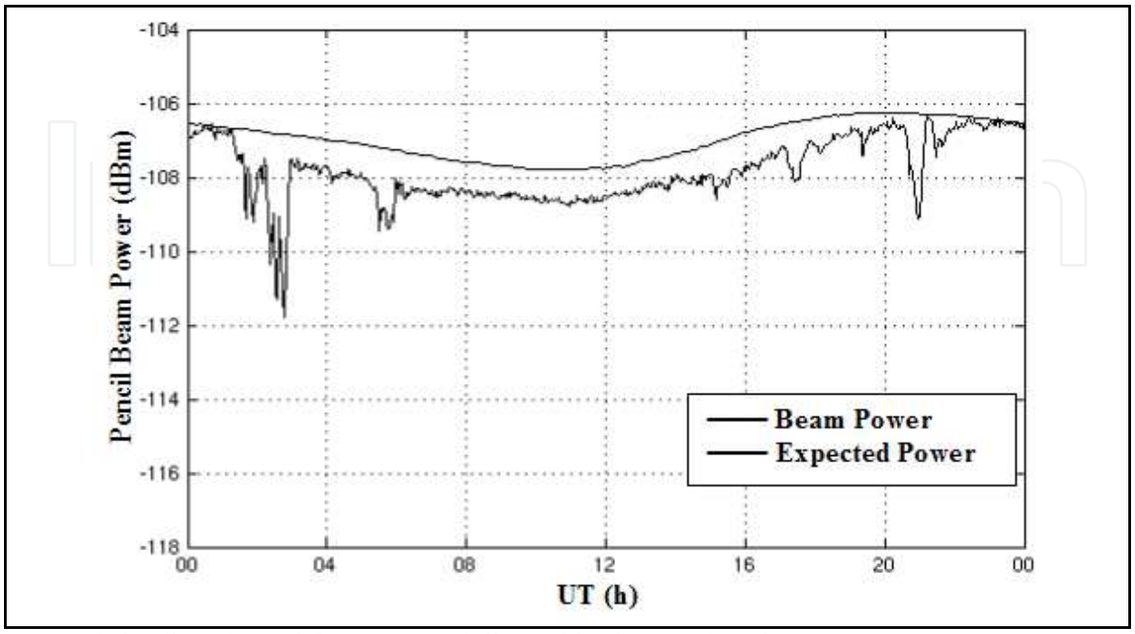

Fig. 13. Solar flare from SGR 1900+14 followed by X-ray afterglows.

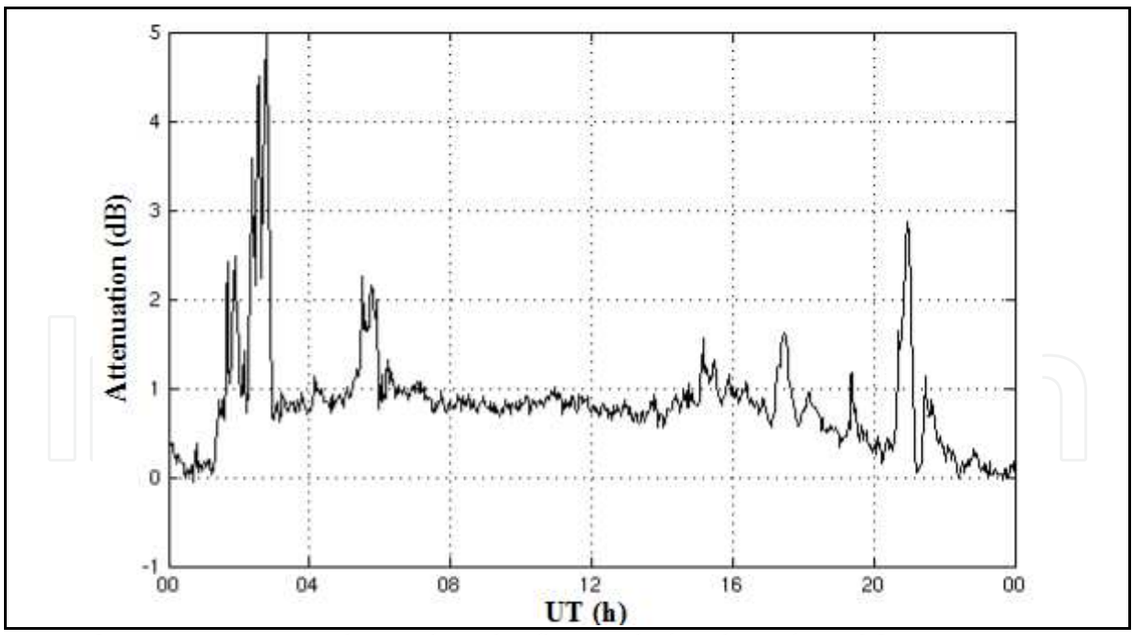

Fig. 14. Strong attenuation, due to the solar flare and afterglows from SGR 1900+14.

Solar activity is categorised in five taxonomies. Level 1 corresponds to less than five unexpected quiet regions. Less than ten class C sub-flares are usually expected, each corresponding to an X-ray blow with peak flux of 1 to 10 angstrom. The transmitted power

is <10 mW/m2. At level 2, less than ten unexpected quiet regions are observed and class C sub-flares are expected. At level 3, solar eruptive regions are observed. The radiation is of class M, with a peak flux of 1-10 angstrom and the power is >10 and <100 mW/m2. At level 4, the active solar regions are responsible for sudden attenuation events. Class M X-ray events can be accompanied by either one or two chromospheric flares. Level 5 involves the highest activity. Protons can be produced in a region on the sun. Class X X-ray burst and several chromospheric flares can occur. Class X X-ray bursts are transmissions over 100 mW/ m2.

Solar radio emissions form four categories. Category I is within 50-300 MHz. Many narrowband, short in period bursts occur. Category II starts at 300 MHz and progressively reduces to 10 MHz. Category II emissions are slightly associated with large solar flares. They consist more of an indication that a shock wave is moving through the solar atmosphere, 676 km/s in Fig. 15. The results of Fig. 15 and 16 are measured at the local plasma frequency, while its harmonics can also be detected. The radiation is similar to that generating the category III bursts.

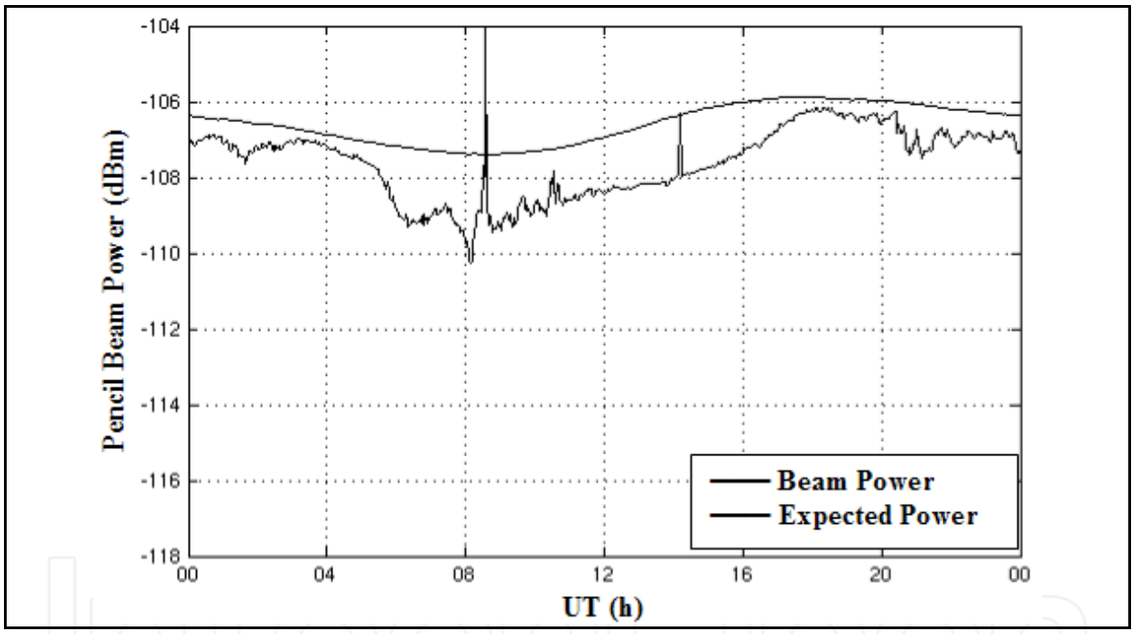

Fig. 15. Category II solar radio emission observed throughout the instrument's operating frequencies.

Two types of shock waves produce the category II radiation. The coronal shocks generate metric bursts and the coronal mass ejection (CME) driven shocks generate interplanetary bursts [15]. Metric category II bursts are related to flares and usually nullify before reaching the high corona. Their relation to Ha Moreton waves verifies that they are generated by blast coronal waves. Moreton waves leave the flare region with speeds in the range of few hundred km/s, e.g. 676 km/s, up to a thousand km/s in other data. Chromospheric trace of magnetohydrodynamic coronal waves generates these bursts.

Category III consists of narrowband bursts that sweep within seconds from decimeter to decameter wavelengths (0.5 to 500 MHz). This category consists of a group of solar

emissions and is a measure of the complex solar active region activity. Category IV is within 30-300 MHz and only broadband bursts occur. These bursts may be associated with major flares 10 to 20 minutes after the flare maximum, and can last for hours.

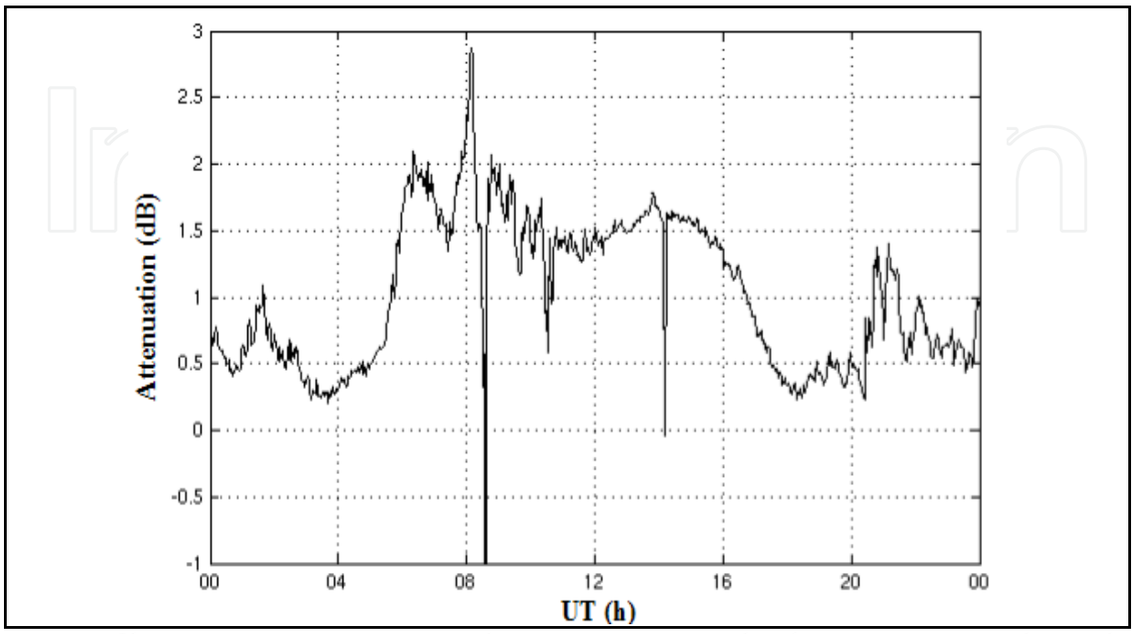

Fig. 16. Characteristic signature on the attenuation results for category II solar radio emissions.

Solar radio emission observations occur during daytime, as in Fig. 15 and 16. They correspond to an increase in the experimental power results. The increased received power is responsible for the large negative attenuation. The emissions' intensity raises concerns to the operation of spaceborne and ground-based instrumentations. The new system automatically adjusts its dynamic range to fully measure the solar radio emissions of categories I - IV. Current and future planetary missions' return-science data would assist in expanding the calculations to other planets and moons.

6. Conclusion

The chapter presents a new reconfigurable wide-beam radio interferometer system for analysing planetary atmospheres. The system operates at frequencies, where the ionisation of the planetary plasma regions induces strong attenuation. For Earth, the attenuation is un-distinguishable from the CMB at frequencies over 50 MHz. The system introduces a set of advanced specifications to this field of science, previously unseen in similar suborbital experiments. The reprogrammable dynamic range of the system expedites signal conditioning to known gain levels to detect Space Physics events. The all-digital architecture facilitates flexible remote control over the numerous programmable or reconfigurable digital functional blocks and external hardware interfaces for fast prototyping of future experiments. The system acts as a pathfinder for future space exploration missions to Luna, Mars, Titan or Europa.

7. References

Abdu, M. A.; Degaonkar, S. S. & Ramanathan, K. R. (1967). Attenuation of galactic noise at 25 MHz and 21.3 MHz in the ionosphere over Ahmedabad during 1957-1964. *Journal of Geophysical Research,* Vol. 72, No. 1, 1574-1554

Bell, A. R.; Gull, S. F. & Kenderdine, S. (1975). New radio map of Cassiopeia A at 5 GHz. *Nature,* Vol. 257, 463-465

Bennett, C. L. et al. (2003). The microwave anisotropy probe mission. *Journal of Astrophysics,* Vol. 583, 1-23

Braine, J. & Hughes, D. H. (1999). The 10 GHz-10 THz spectrum of a normal spiral galaxy. *Journal of Astronomy and Astrophysics,* Vol. 344, No. 1, 779-786

Haldoupis, C. I. et al. (1982). Radar auroral observations during a burst of irregular magnetic pulsations. *Journal of Geophysics,* Vol. 87, No. A3, 1541-1550

Hargreaves, J. K. (1995) *The solar-terrestrial environment,* Cambridge University Press

Hinsaw, G. et al. (2008). Five-year microwave anisotropy probe (WMAP) observations: data processing, sky maps, & basic results. *Journal of Astrophysics,* Vol. x, xx-xx

Kelsall, T. et al. (1998). The COBE diffuse infrared background experiment search for the cosmic infrared background. II. model of the interplanetary dust cloud. *Journal of Astrophysics,* Vol. 508, No. 1, 44-73

Lamarre, J. M. et al. (2003). Planck high-frequency instrument. *Proceedings SPIE 4850,* pp. 730-739

Le Vine, D. M. & Abraham, S. (2004). Galactic noise and passive microwave remote sensing from space at L-band. *IEEE Transactions of Geoscience and Remote Sensing,* Vol. 42, No. 1, 119-129

Mather, J. C.; Richards, P. L. & Woody, D. P. (1974). Balloon-based measurements of the cosmic background radiation. *IEEE Transactions of Microwave Theory and Technology,* Vol. 22, No. 12, 1046-1048

Pinto, J. O. & Gonzalez, W. D. (1989). Energetic electron precipitation at the South Atlantic magnetic anomaly: a review. *Journal of Atmospheric and Terrestrial Physics,* Vol. 51, No. 5, 351-365

Pui-In, M.; Seng-Pan, U. & Martins, R. P. (2007). Transceiver architecture selection: review, state-of-the-art survey and case study. *IEEE Circuits and Systems Magazine,* Vol. 7, No. 2, 6-25

Reber, G. & Ellis, G. R. (1956). Cosmic radio-frequency radiation near one megacycle. *Journal of Geophysical Research*, Vol. 61, No. 1, 1-10

Rzhiga, O. N. (2005). Distortions of the low frequency signal by Martian ionosphere at vertical propagation. *IEEE Transactions of Antennas and Propagation,* Vol. 53, No. 12, 4083-4088

Thomson, A. R.; Moran, J. M. & Swenson, G. W. Jr. (2001). *Interferometry and synthesis in radio astronomy,* Wiley-Interscience

Stoker, P. H. et al. (1997). Cosmic radio noise absorption related to structures in aurora luminosity. *Journal of Geophysical Research,* Vol. 102, No. A4, 7439-7447

Wilson, R. W. (1979). The cosmic microwave background radiation. *Revision of Modern Physics,* Vol. 51, No. 3, 433-446

Air Pollution

Edited by Vanda Villanyi

ISBN 978-953-307-143-5

Hard cover, 370 pages

Publisher Sciyo

Published online 17, August, 2010

Published in print edition August, 2010

Although the climate of the Earth is continually changing from the very beginning, anthropogenic effects, the pollution of the air by combustion and industrial activities make it change so quickly that the adaptation is very difficult for all living organisms. Researcher's role is to make this adaptation easier, to prepare humankind to the new circumstances and challenges, to trace and predict the effects and, if possible, even decrease the harmfulness of these changes. In this book we provide an interdisciplinary collection of new studies and findings on the score of air pollution.

InTech Europe

University Campus STeP Ri
Slavka Krautzeka 83/A
51000 Rijeka, Croatia
Phone: +385 (51) 770 447
Fax: +385 (51) 686 166
www.intechopen.com

InTech China

Unit 405, Office Block, Hotel Equatorial Shanghai
No.65, Yan An Road (West), Shanghai, 200040, China
中国上海市延安西路65号上海国际贵都大饭店办公楼405单元
Phone: +86-21-62489820
Fax: +86-21-62489821

IntechOpen